Space charge in liquid ionization detectors

Sandro Palestini, CERN

CERN Detector Seminar, 12 May 2023

Introduction: space charge in ionization detectors

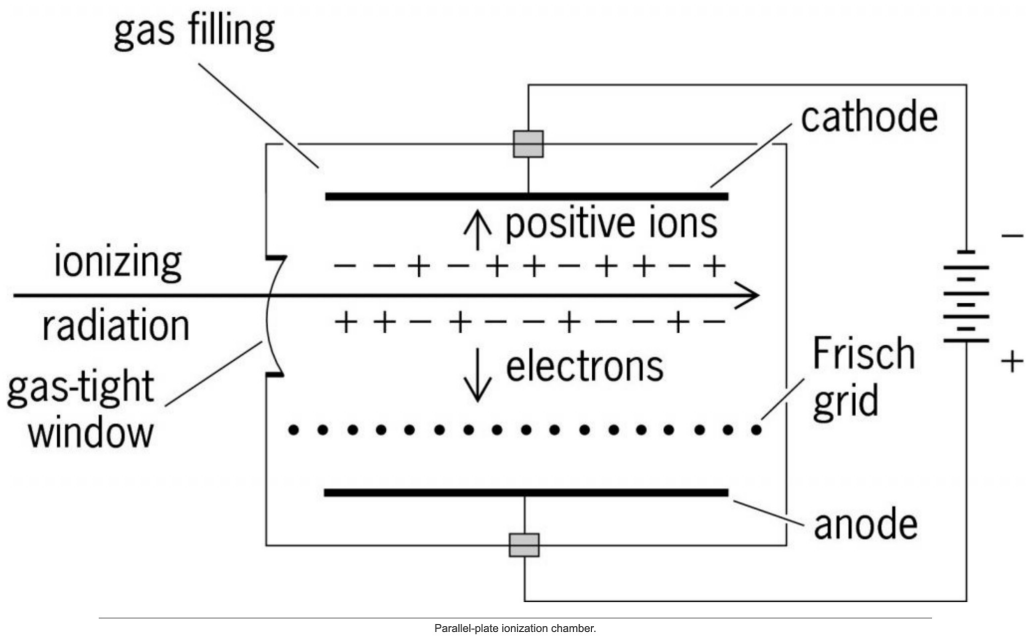

Parallel-plate ionization chamber.

- Ionization (parallel plate) chamber as illustrated by an image from a Google search.
- Generally fine, but the length of the arrows should not be taken as suggestive of the drift velocities of electrons and positive ions:
  - The velocity of the ions may be about 10^6 times lower than electrons
  - If the irradiation is sufficiently high,
  - or if the gap length is sufficiently long,

  the positive charge density stored in the detector may be comparable to the charge on the electrode, and in that case the response of the detector is affected.

- In gaseous detector with charge multiplication, ions are produced mainly in the multiplication process. Ion gates have been used to collect them, preventing them from entering the drift volume.
- We shall not discuss that, but we shall consider liquid noble element detectors (liquid krypton, liquid argon).
- We shall start with calorimeters, for historical reasons and in order to present the basic formalism that was developed to describe space charge effects and specify critical conditions.
- Then we shall discuss large TPCs for neutrino detectors, where space charge from cosmic rays may be sufficient to cause large effects, and where additional features are related to detector boundaries.

Content

- Introduction
- Calorimeters
  - NA48: geometry, evidence of space charge
  - 1-D simple model for space charge
  - Space charge limited conditions in configurations similar to ATLAS FCAL.
- LAr TPCs for neutrino experiments
  - Detector geometry and relevance of cosmic ray flux
  - Longitudinal (drift direction) space charge effect
  - Transversal effects
  - Transversal effects as boundary mismatch, mitigation via field cage
  - Mitigation via interposed grid
  - Dual phase TPC with gas gain: critical conditions
  - Liquid krypton TPCs ?
  - The additional complexity of fluid motion
  - Calibration methods.

The NA48 calorimeter

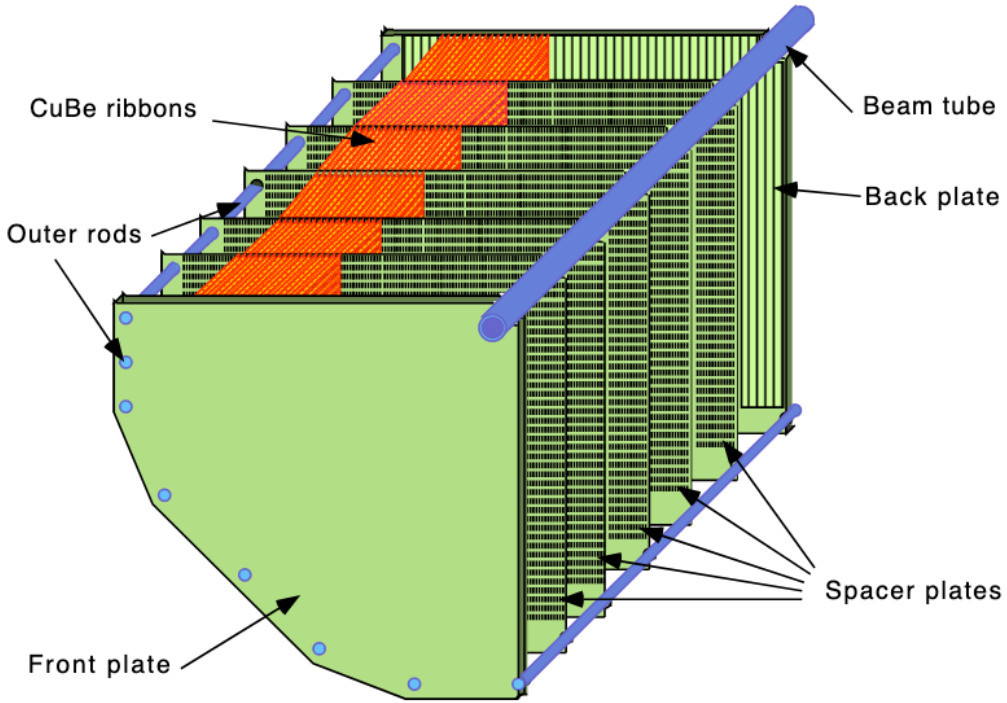

Figure 1. A quadrant of the electrode structure.

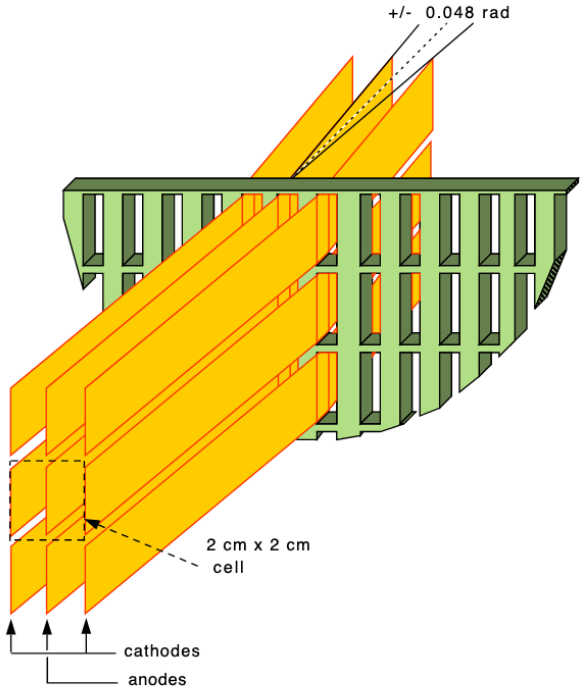

Figure 2. Detail of ribbon electrodes near a spacer plate.

A quasi homogeneous liquid krypton calorimeter, with longitudinal readout cells, operated at rather high intensity in the CERN North Area. Actually, still operated 26 years later, for the NA62 experiment.

The NA48 calorimeter -2

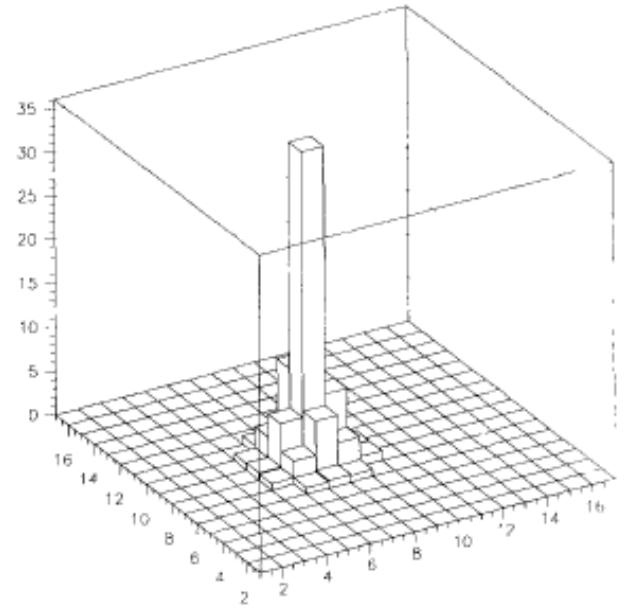

Fig. 10. Typical shower profile as measured with 120 GeV electrons.

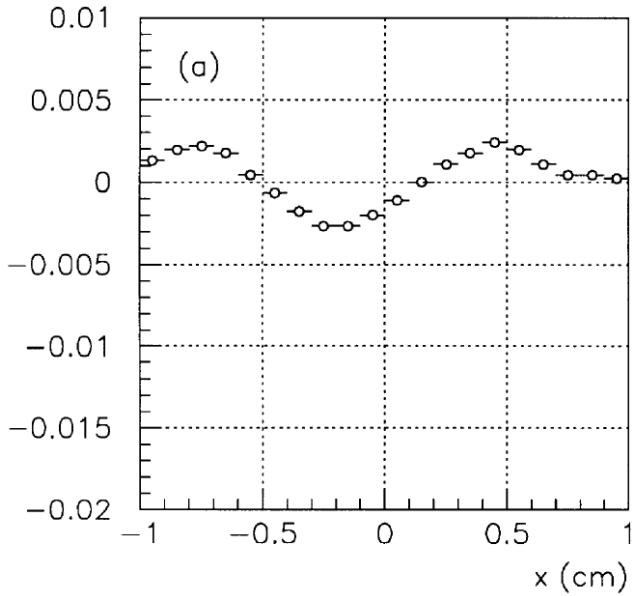

Fig. 16. Non–uniformity of detector response at low intensity (a)

The orientation of the readout, together some passive material and limited readout bandwidth in the initial current readout, generate some modulation in the detector response vs. the position of the shower axis within the readout grid.
The accordion geometry defines a smooth, asymmetric behaviour of this dependence.

The relevance of space charge occurred for a kind of accidental reason: in 1997, for the first physics run, the bias voltage was set at 1.5 kV (with 1 cm gap), rather than 3 kV, the design value used in the following years, which causes much smaller space charge effects.

Space charge evidence in NA48

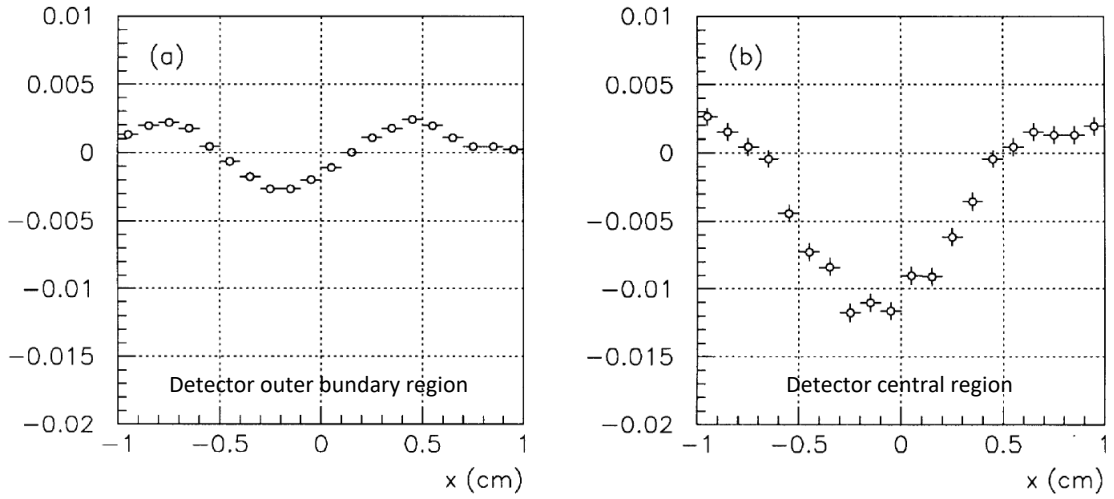

Fig. 16. Non–uniformity of detector response at low intensity (a) and at high intensity (b).

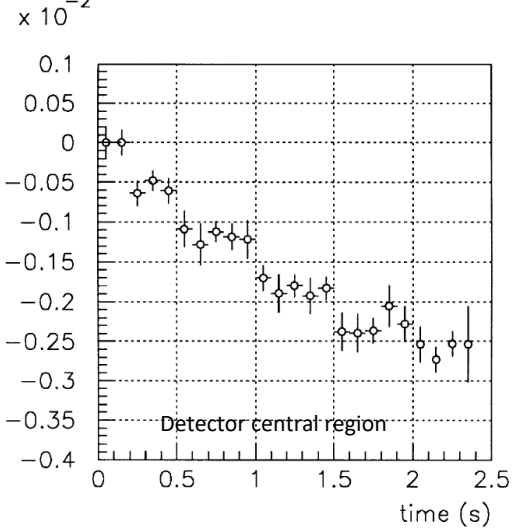

Fig. 10. Dependence of the response of the NA48 calorimeter on the shower time within the SPS extraction period.

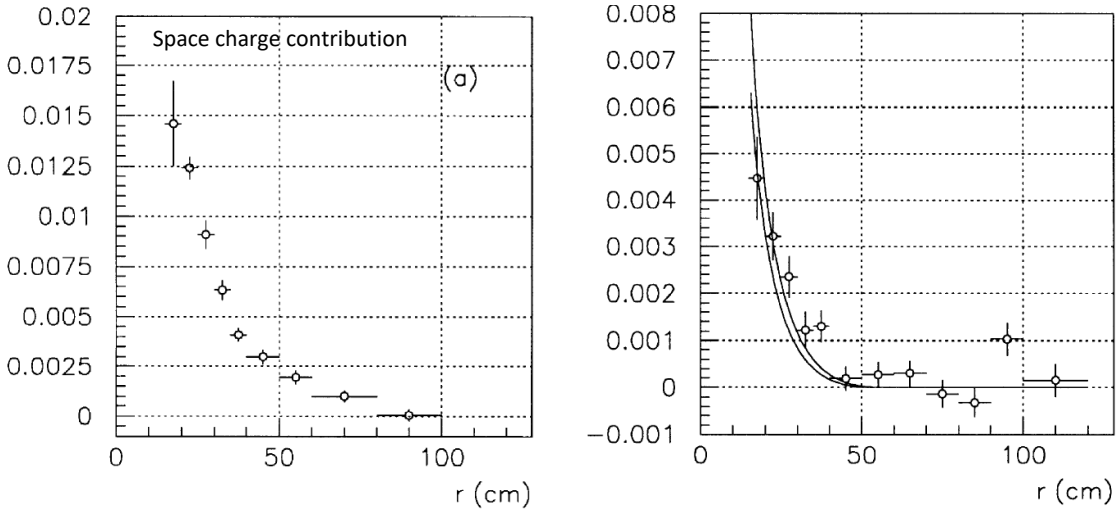

g. 17. Dependence of the peak-to-peak modulation of the response on the radial position (a)

Fig. 15. Measured average reduction of response (data points) compared to the prediction.

- The observed effects are correlated with the irradiation profile on the detector face (r dependence),
- with the position of the shower axis within the central cell of the shower cluster (x dependence, hence E(x) dependence)
- and with the time within the beam extraction cycle (t dependence): the space charge increases during the first ≅ 1.5 s of the spill, then stays constant, then is disposed before the next spill.

  All features, including an normalization to the spill intensity measured by beam monitors, were included in data calibration.

The basic, 1D model for space charge

With the assumption that the charge density of the electrons is negligible, the basic model is simple:

- Charge continuity equation:

  $$\frac{\partial \rho^+}{\partial t} + \frac{\partial (\rho^+ v_x^+)}{\partial x} = K$$

  K is the charge density injection rate

- Stationary solution, with ion velocity $v_x^+ = \mu^+ E_x$:

  $$\rho^+(x) = \frac{K x}{\mu^+ E(x)}$$

  x=0 on the anode.

- Use Gauss equation: $\frac{dE_x}{dx} = \frac{\rho^+}{\varepsilon}$

- And solve for E_x(x) as : $E_x(x) = E_\circ \sqrt{(E_a/E_\circ)^2 + \alpha^2 (x/L)^2}$

  where E_a is the field at the anode determined by the boundary condition : $\int E_x dx = V_\circ = E_\circ L$

  and the dimensionless parameter α is $\alpha = \frac{L}{E_\circ}\sqrt{\frac{K}{\varepsilon \mu^+}}$

The amplitude of space charge effects is proportional to α^2, which can be described as the ratio of charge injection rate, multiplied by the drift gap and by the nominal maximum ion drift time, divided by the nominal charge density on each electrode: $\alpha^2 = K\, L\, (L/\mu^+ E_0) / (\varepsilon\, E_0)$.

Basic model - II

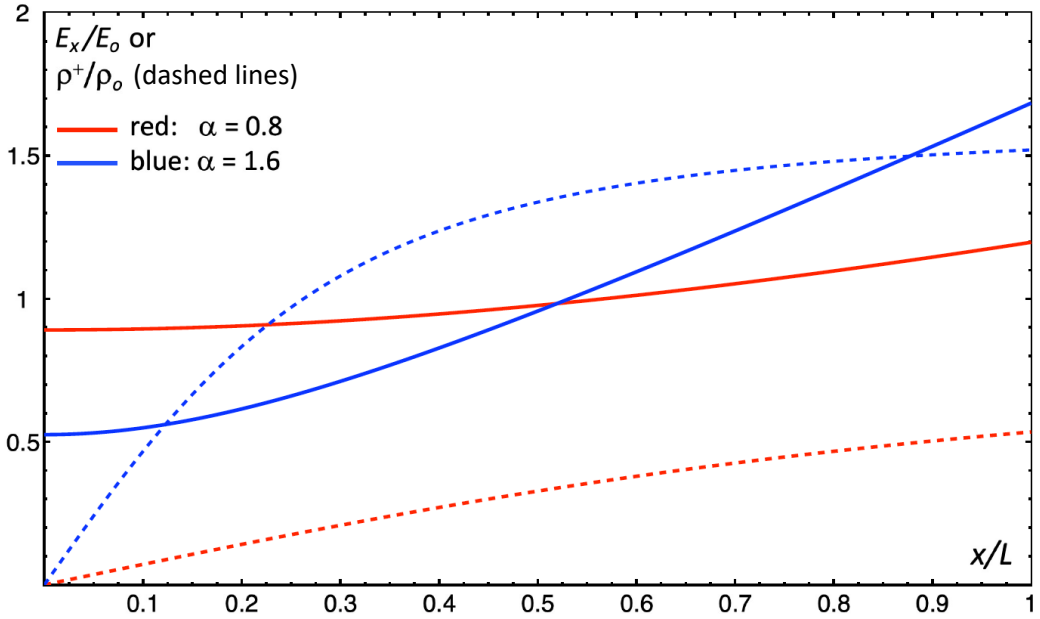

Normalized E field and normalized space charge density ($\rho_0 = \varepsilon E_0/L$), vs. normalized coordinate *x*, anode to cathode.

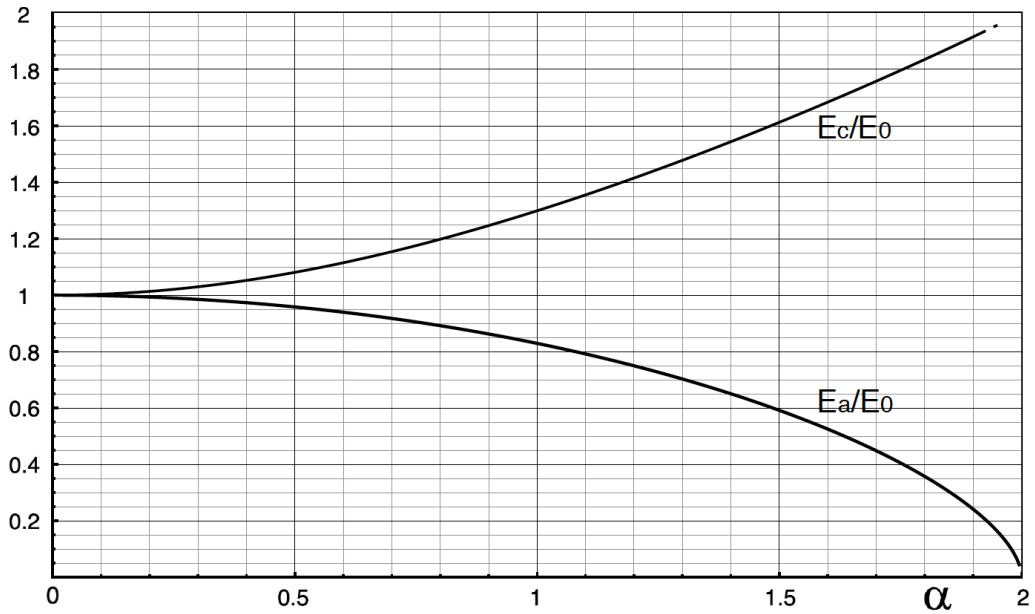

Value of the E field at the electrodes, as a function of the parameter α.

$0 < \alpha < 2$

- The electric field strength is reduced at the anode, increased at the cathode.
- The non uniformity of E(x) is the reason for the increased response variation with the position of the shower axis within the cell, seen in NA48 (effective value for e.m. showers $\alpha = 1.1$ on inner radial boundary).
- The small reduction seen in average amplitude is due the convexity of the the electron drift velocity $v_e(E)$, as E(x) varies between E_a and E_c (the loss of signal in the anode region is effectively larger than the gain at the cathode).

Basic model - III

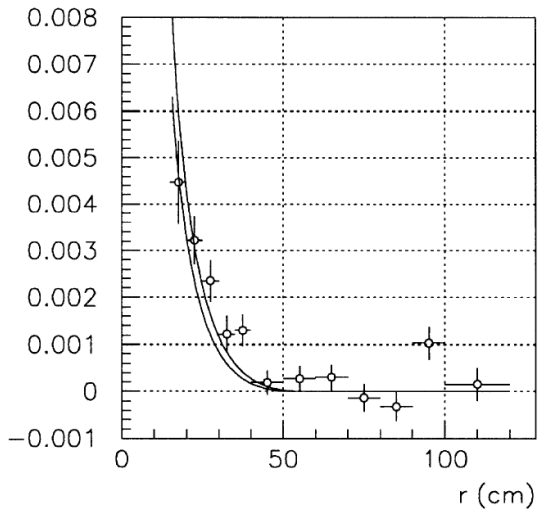

Fig. 15. Measured average reduction of response (data points) compared to the prediction.

The curves are not a fit, but a prediction only based on energy flow estimate and on the value of the the ion mobility derived fron the onset time of ≅1.5 s.

How does the time dependent solution look like?

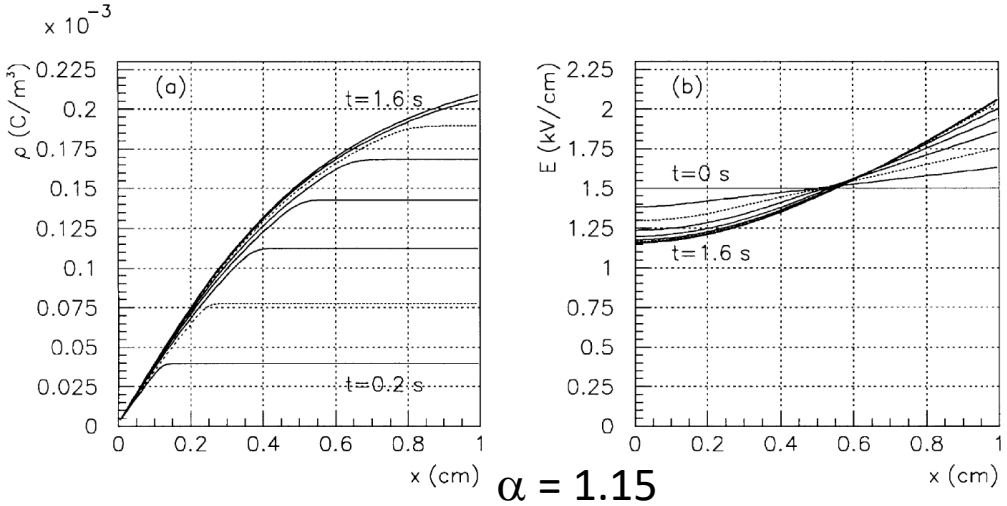

α = 1.15

Fig. 2. Space charge density and (b) electric field vs. x, for different time values during the charge injection interval, for $\alpha = 1.15$.

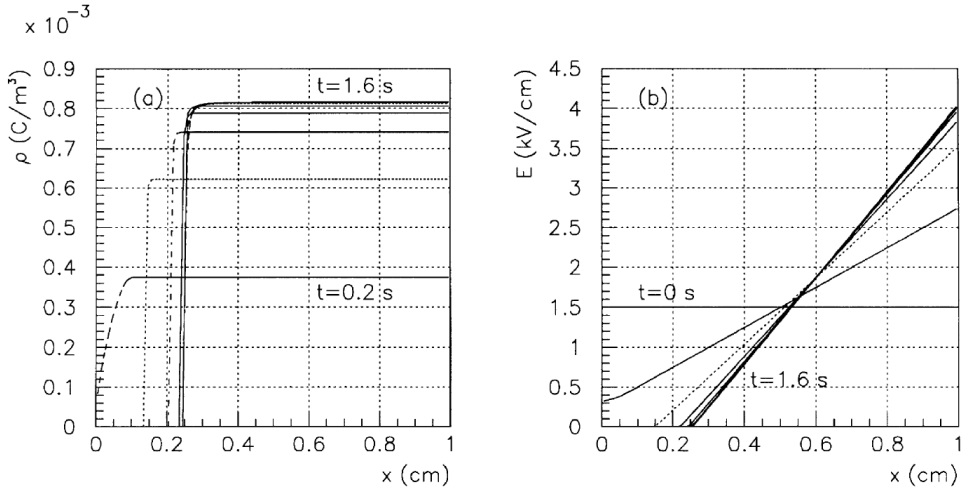

Fig. 4. Same as Figs. 2 and 3 but with $\alpha = 3.6$. The *contraction parameter* is $\xi = 0.74$.

α = 3.6

The description of the basic model fails for $\alpha > 2$, since the field at the anode cannot become negative.

A direct extension suggests that the field and the ions density would vanish in a region near the anode.

This picture cannot be accurate, but very likely the electron signal is significantly reduced in that situation.

This has been the subject of studies by others, in more recent years.

Liquid argon calorimetry R&D for ATLAS HL-LHC operation

[J. Rutherfoord et al., U. Arizona]

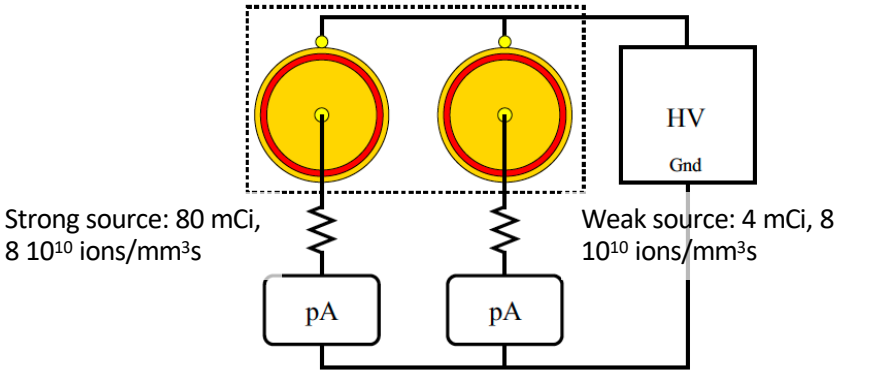

Strong source: 80 mCi, 8 10^{10} ions/mm^{3}s

Weak source: 4 mCi, 8 10^{10} ions/mm^{3}s

For comparison: ATLAS FCAL at η=4.7 : 6 10^{10} ionisation mm^{-3}s^{-1} at shower maximum, luminosity 1 10 ^{34} cm^{-2} s^{-1}, 22kV/cm, gap similar to intermediate configuration of this test.

Three gaps configurations: 0.14, 027, 0.90 mm

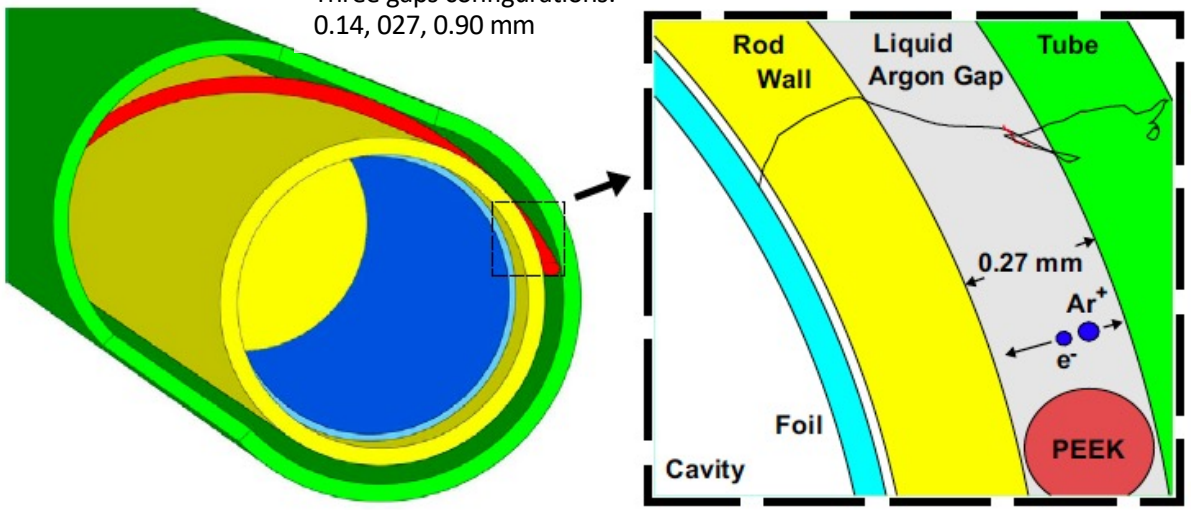

The detectors are similar to components in the Forward Calorimeter of ATLAS:
ionisation chambers built as cylindrical shells.

Thres configurations of different, sub-mm gaps.

Two detector, equipped with ^{90}Sr sources, were used, comparing the current drawn in the two.

The source intensities could not be varied, but the onset of “space charge limited” conditions was studied by varying the bias voltage, from 2 kV down to a few V.

In this regime, initial recombination and long distance (uncorrelated) recombination were modelled.

R&D for ATLAS HL-LHC - II

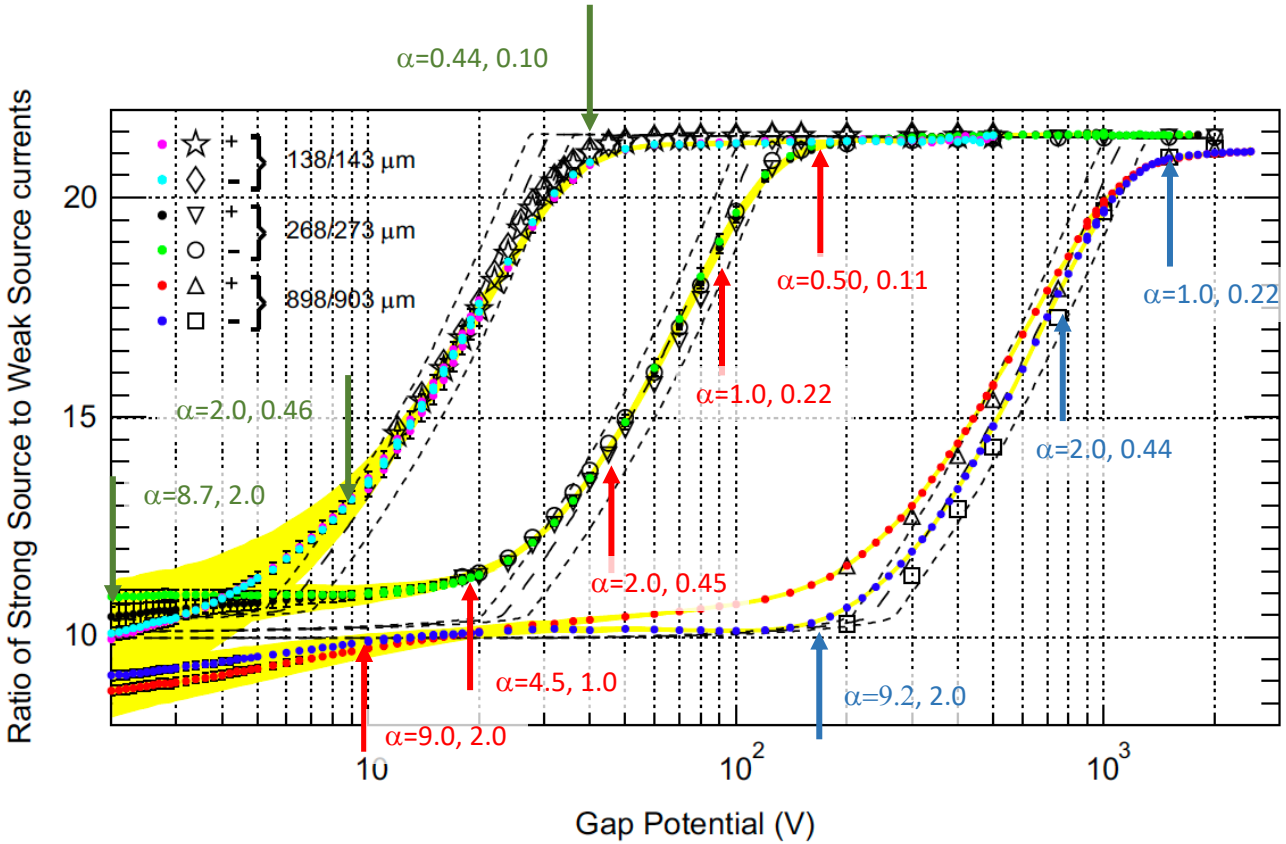

Arrows and values provide values of α parameter for the strong and weak sources, respectively. The onset of space charge limited condition occurs at values $\alpha \cong 1$ for the largest gap, $\alpha \cong 0.5$ for the other.

Results: for each of the the three configuration of gap width, at high values of the bias voltage, the two chambers respond proportionally to the ratio of the sources activities.

Lowering the voltage, there is first a transition in which the detector with the strong source reduces its response (this happens at about 1000, 100, and 30 V, respectively for the three gaps of 0.90, 0.27 and 0.14 mm).

Next, also the detector with weaker source becomes response limited (at about 200, 20 and 4 V, respectively). The data is in fair agreement with the simulation, which is substantially basic model plus recombination effects, for an ion mobility fitted value of 0.08+-0.02 $mm^2\ V^{-1}\ s^{-1}$.

Liquid argon time projection chambers (ProtoDUNE)

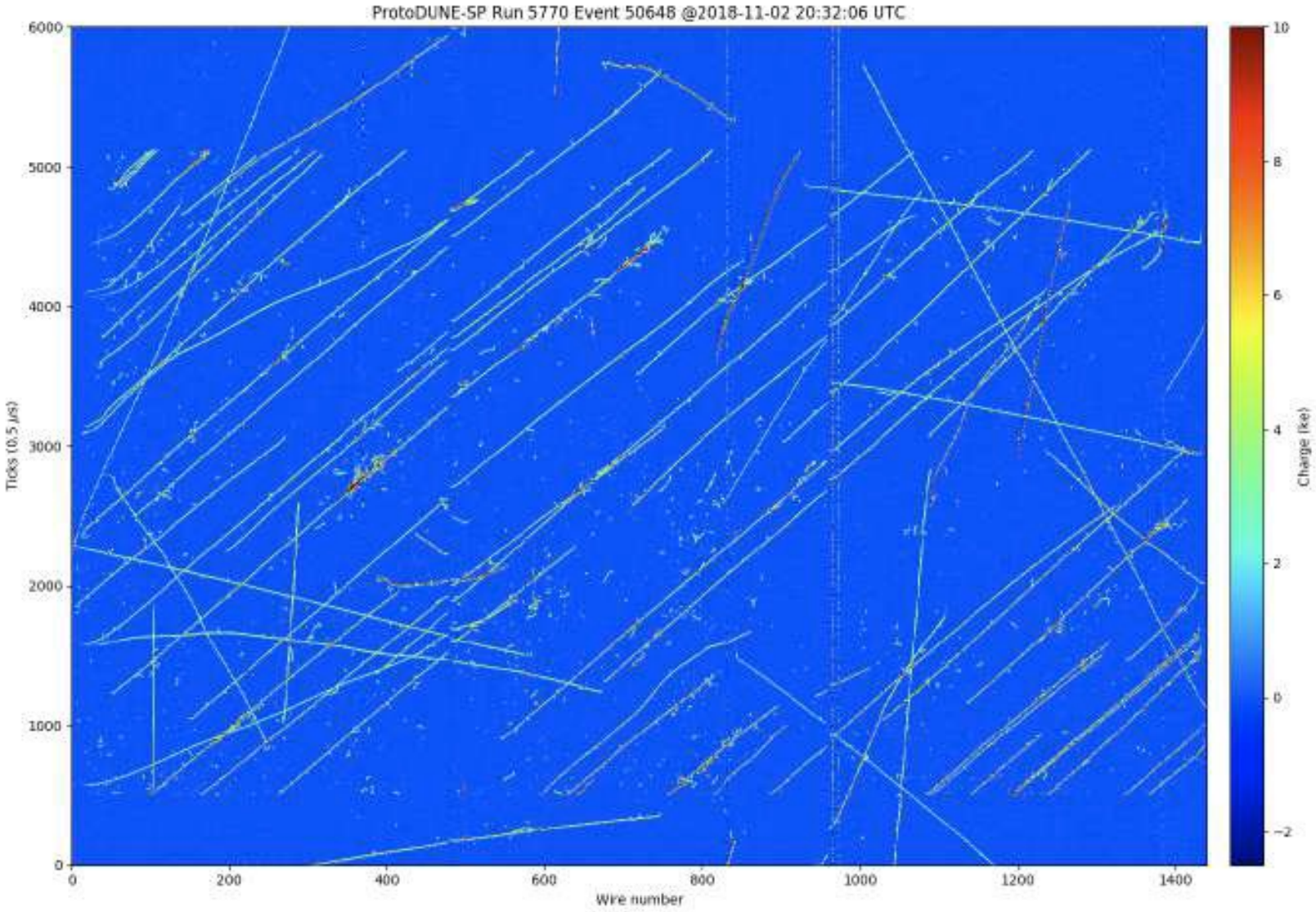

Shower of cosmic ray muons in one of the drift volumes of ProtoDUNE Single-Phase (horizontal drift) detector.
The image covers 7 meters
times 2.3 ms = 3.6 m along the drift direction.

LAr TPCs

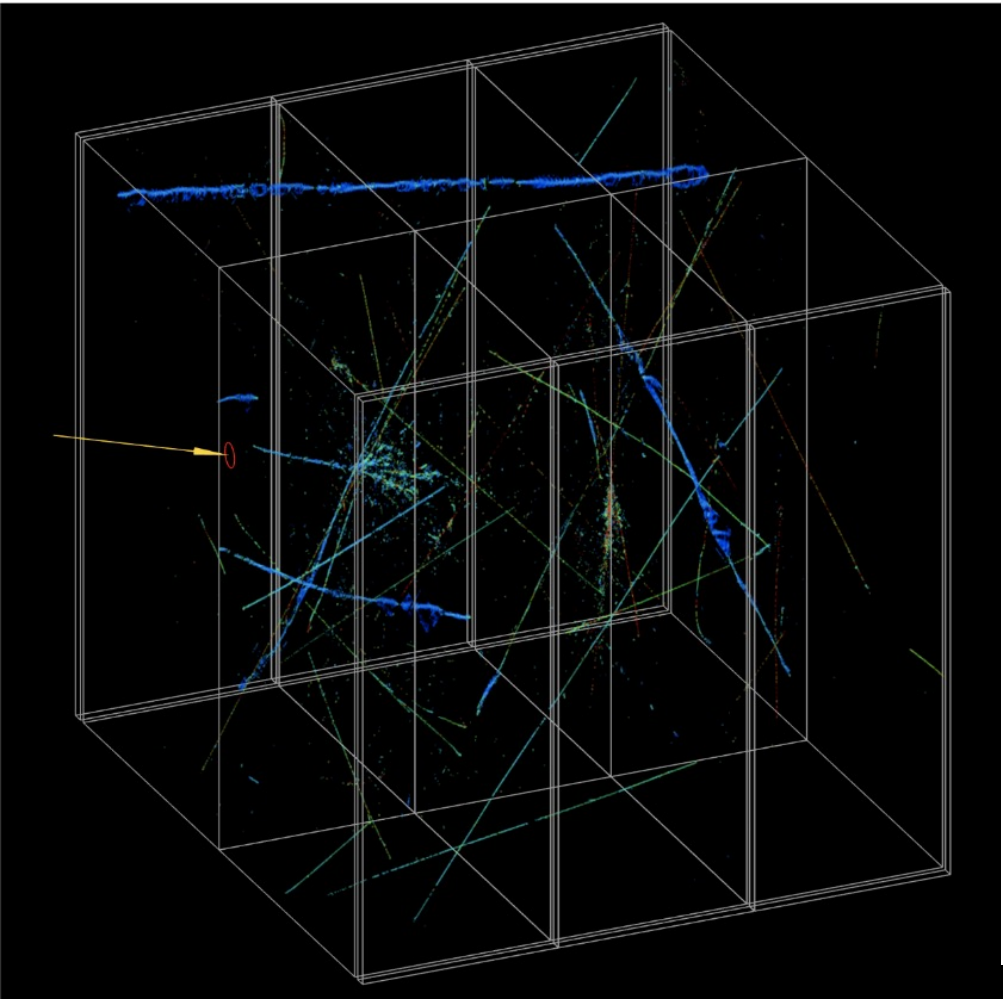

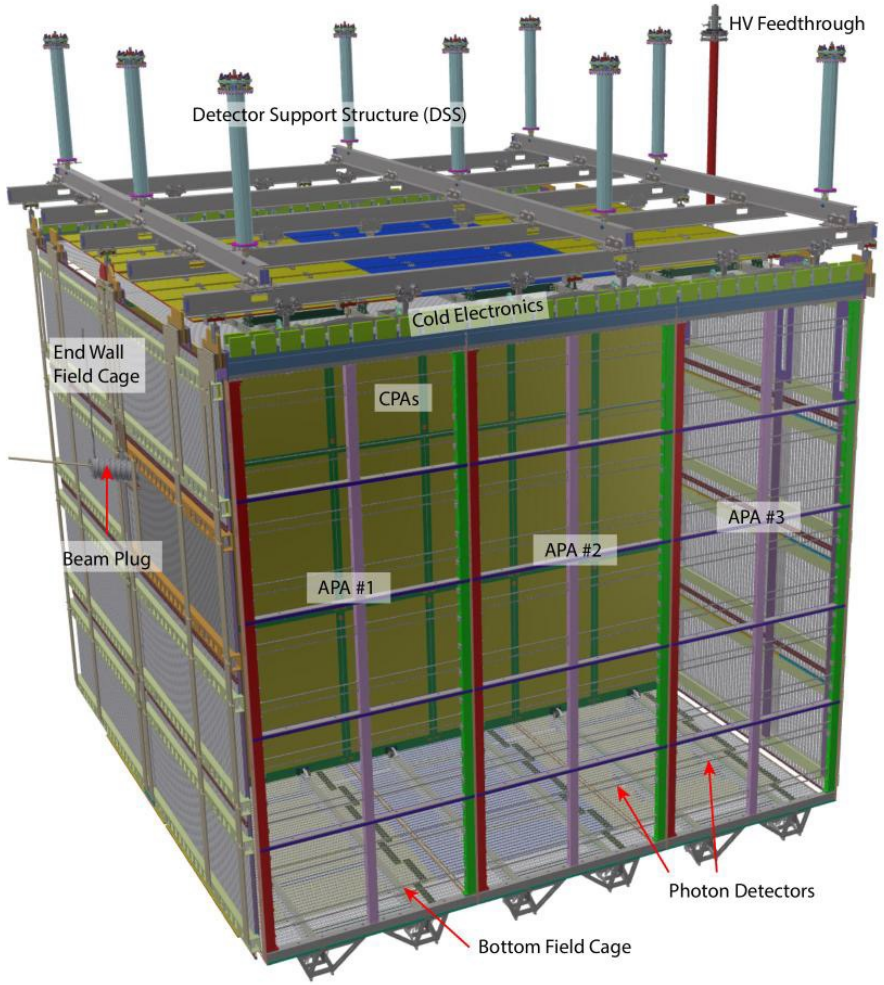

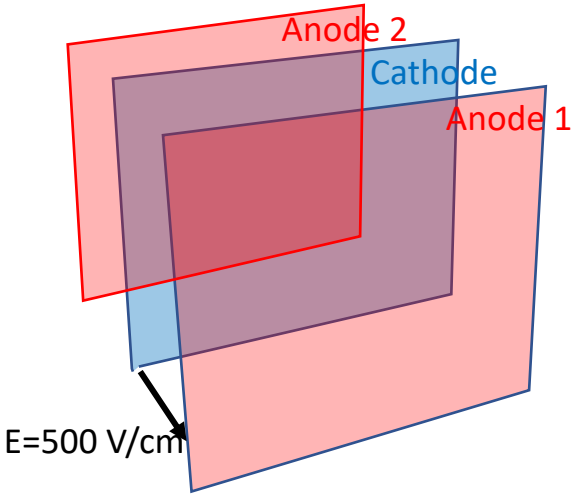

3D reconstructed event in ProtoDUNE-SP, showing beam particle interaction and overlay of cosmic ray signals.

Calorimeter vs. LAr TPCs on Earth surface

Compare $\alpha^2 = \frac{L^2 K}{E^2 \mu\varepsilon}$

$\mu\varepsilon$ Permittivity and ion mobility values are comparable

$\frac{L^2}{E^2}$ NA48 (1997) central region: (1 cm/1.5 kV/cm)^2 = 0.44 cm^{4}kV^{-2}

ProtoDUNE-SP: (360 cm/0.5 kV/cm)^2 = 518 k cm^{4}kV^{-2}

different by factor ~ 1.2 x 10^6

K NA48 central region: 130 pC cm^{-3}s^{-1}

Cosmic rays in liquid argon: 200 pC m^{-3}s^{-1}

different by factor ~ 1.5 x 10^{-6}

Despite the huge differences in the separate contributions, in the combination the situation is similar:

NA48 had $\alpha \cong 1.1$ (central region)

ProtoDUNE-SP has $\alpha \cong 0.7$

Other LAr TPCs:

ICARUS (on surface) $\alpha \cong 0.4$

MicroBooNE $\alpha \cong 0.8$

SBND shoudl have $\alpha \cong 0.5$

SC effects in LAr TPC 1: distortion in drift coordinate (ICARUS)

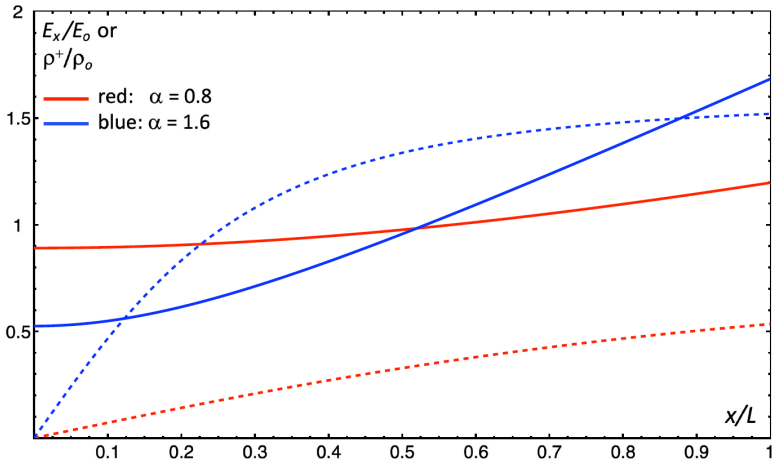

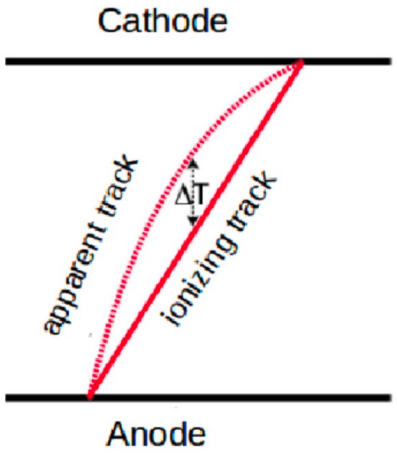

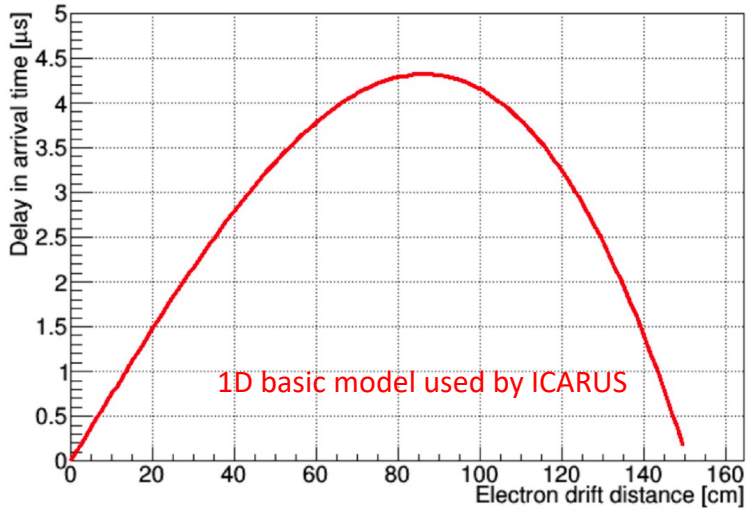

The drift velocity is higher near the cathode, and lower near the anode, because of the change in E field due to space charge.

The effect on the drift time is null on anode and about so also cathode (in the approximation $\langle 1/E(x) \rangle \cong 1/\langle E(x) \rangle = 1/E_0$).

The resulting distortion occurs in the central region of the detector, visible on tracks with some inclination to the drift direction. Rather small in ICARUS (on surface – no effects underground in LNGS), larger (some cm) in MicroBooNE and ProtoDUNE-SP.

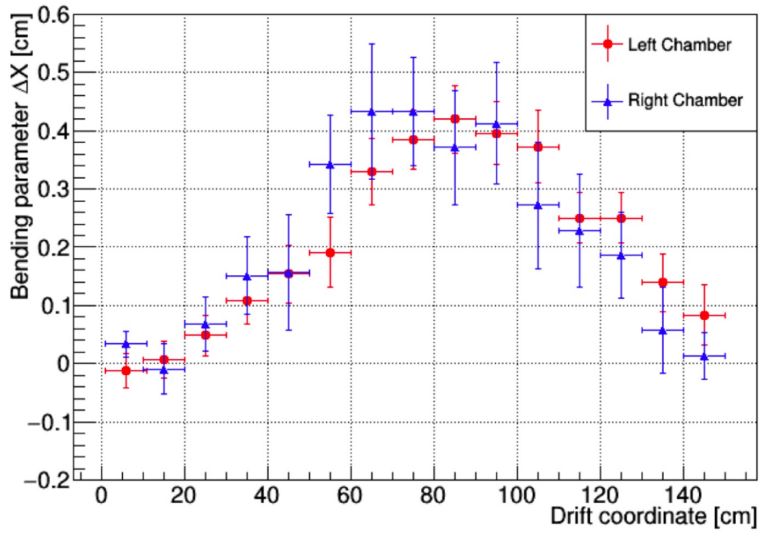

Additional effect in TPCs

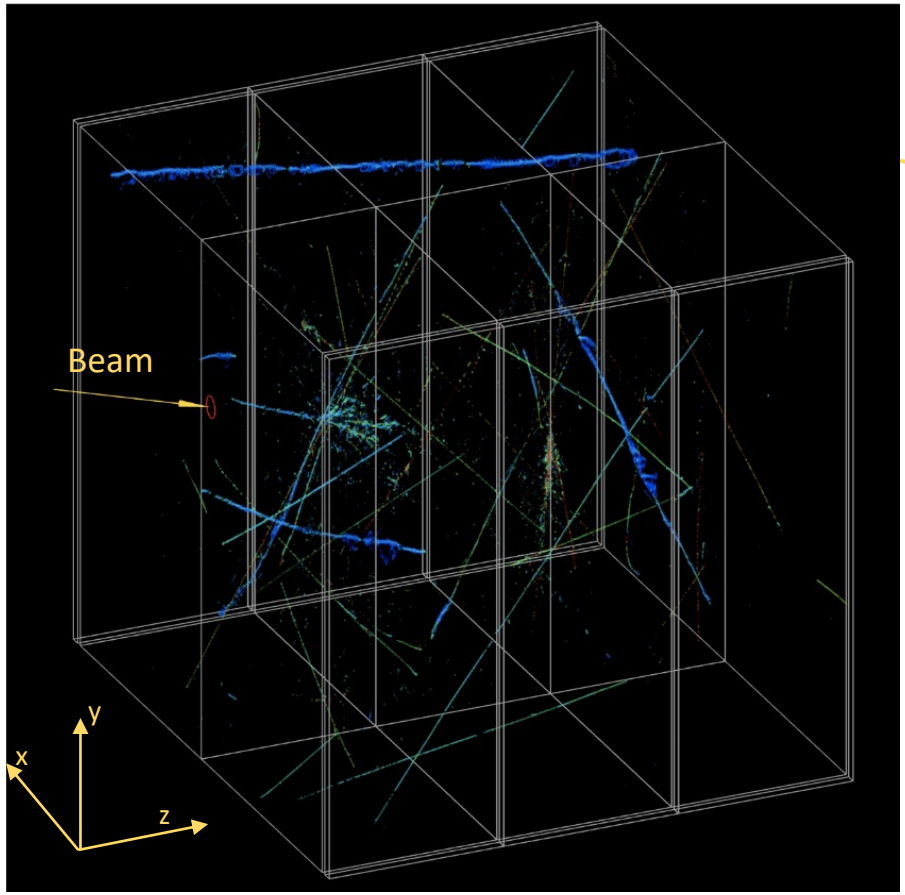

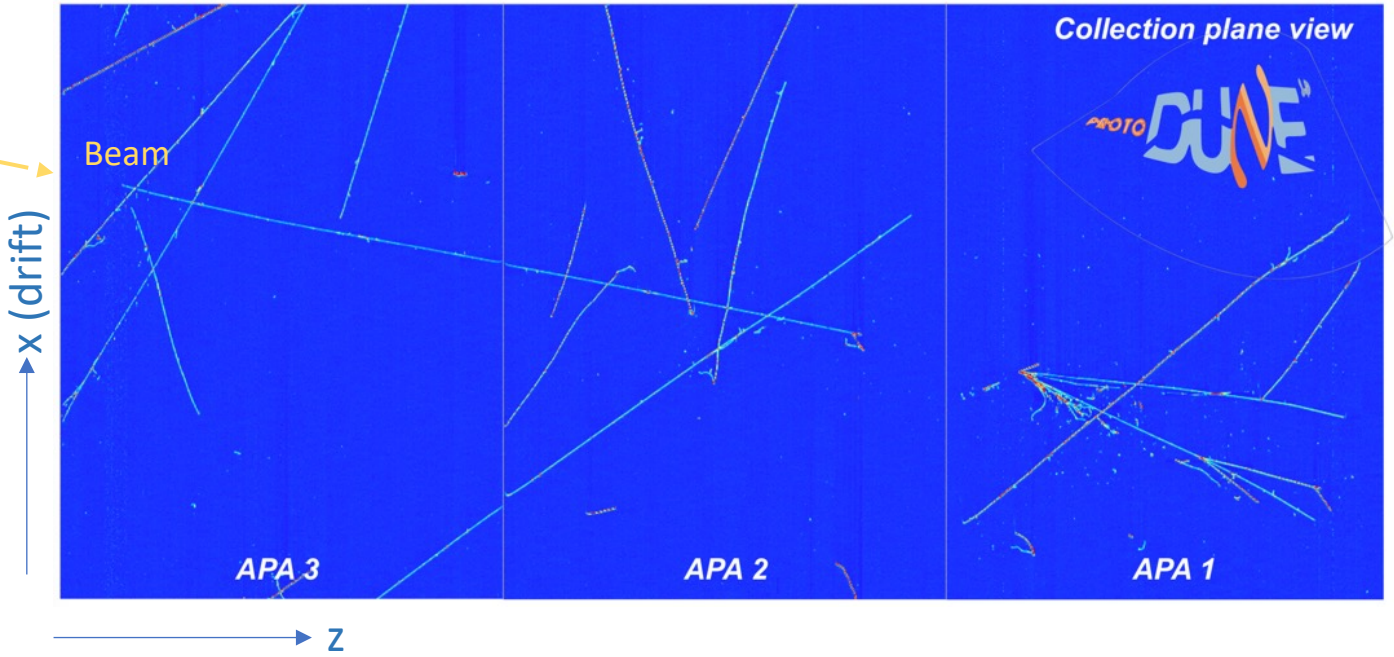

The apparent entrance point of the beam particle is inside of the active volume.
This does not happen for entrance/exit points of other tracks.

Transversal distortion in TPCs

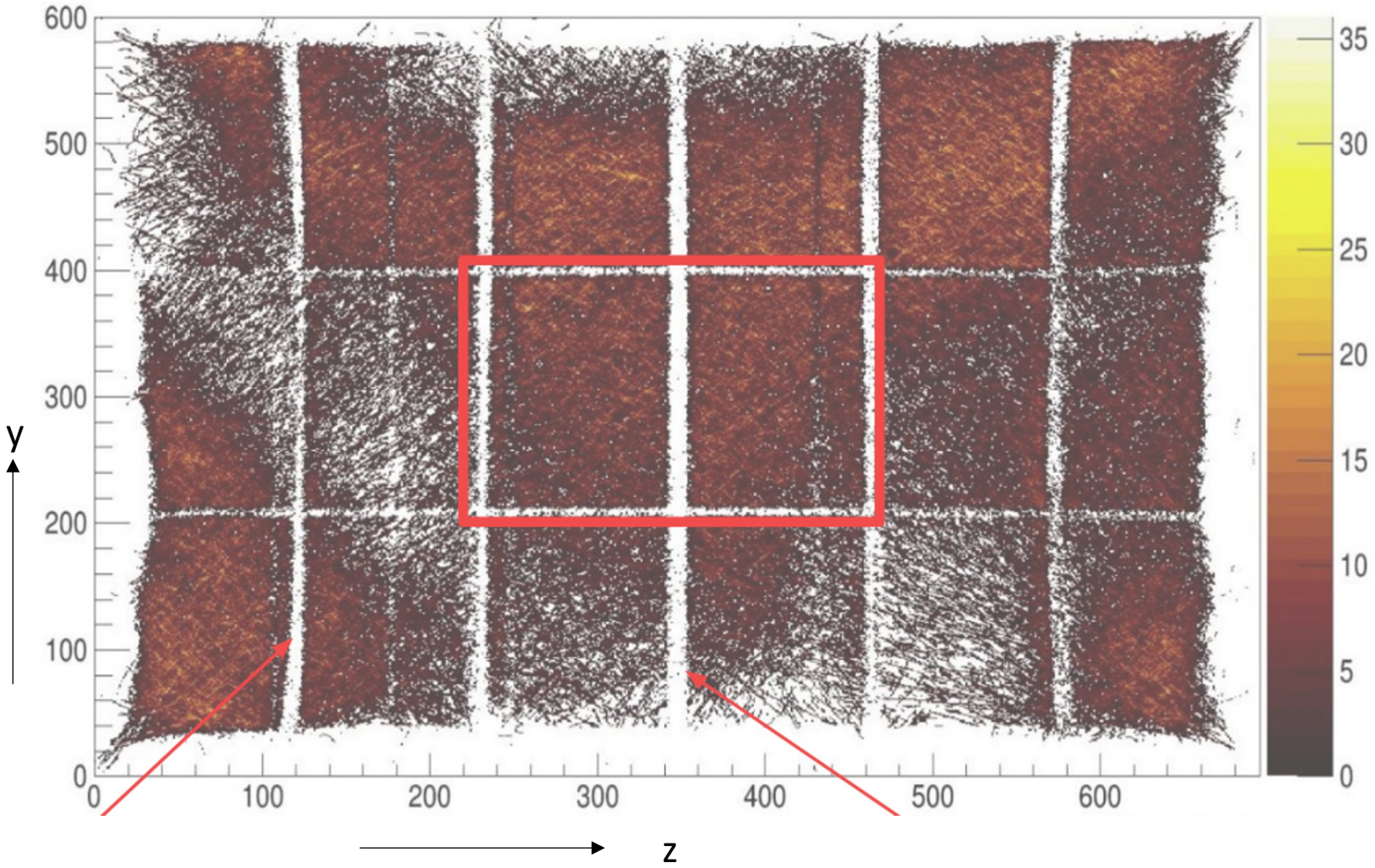

ProtoDUNE-SP:

Transversal coordinates of cathode crossing points of cosmic rays.

The empty bands are mechanical support structure of the cathode that alter the electric field in its proximity – and alter the path of ionization electrons from that region.

There is lensing (pin-cushion) effect near boundaries, i.e. near the field-cage. No distortion in the detector bulk volume.

Transversal effects in TPCs

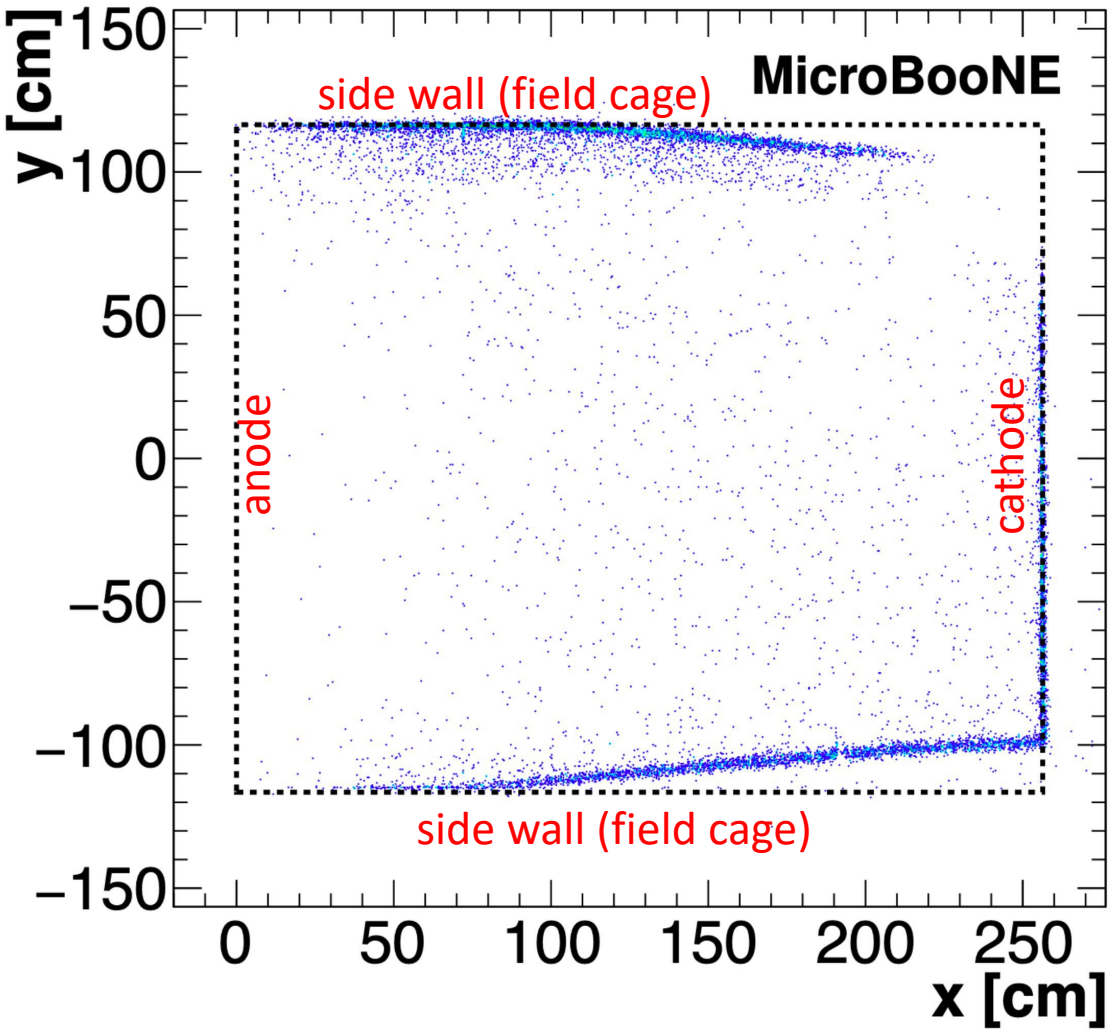

Here is how the effect is seen in MicroBooNE, this time looking at the transversal coordinate on which particles cross the boundaries of the active volume:

The effect vanishes near the anode, and is large near the cathode (~ 10 cm, larger than longitudinal effects).

In fact, drifting eletrons experience a same-sign transversal effect all along their drift to the anode, while the longitudinal effect has different sign in the cathode and anode regions.

Sometimes people say that *ionisation electrons drifting near the boudaries are attracted inward by the space charge on the inside of the active volume*.

This statement neglects that whenever there is space charge in the detector volume, the distribution of charge is modified on the entire boundary. Better to describe it as a *mismatch of boundary conditions*.

Side boundary effects

Equipotential surfaces with s.c. distortion,
α = 0.8 , far from side boundaries

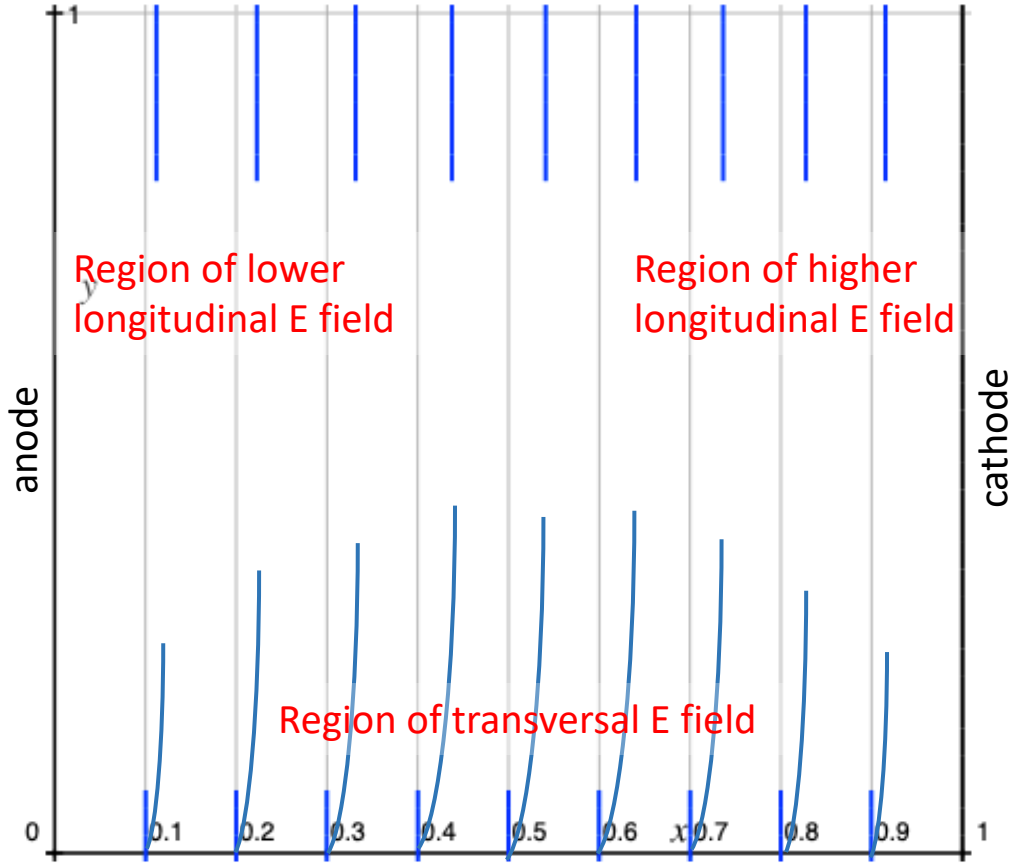

Equipotential surfaces defined by nominal field cage

Far from side boundaries, the elecric field is defined by the space charge,

while on the field cage, usually the nominal voltage gradient is imposed.

The transition between the two region generates a transversal component in the E field, outward directed.

A non-linear field cage gradient can change the situation.

Reducing the transversal effect with the field cage voltage gradient

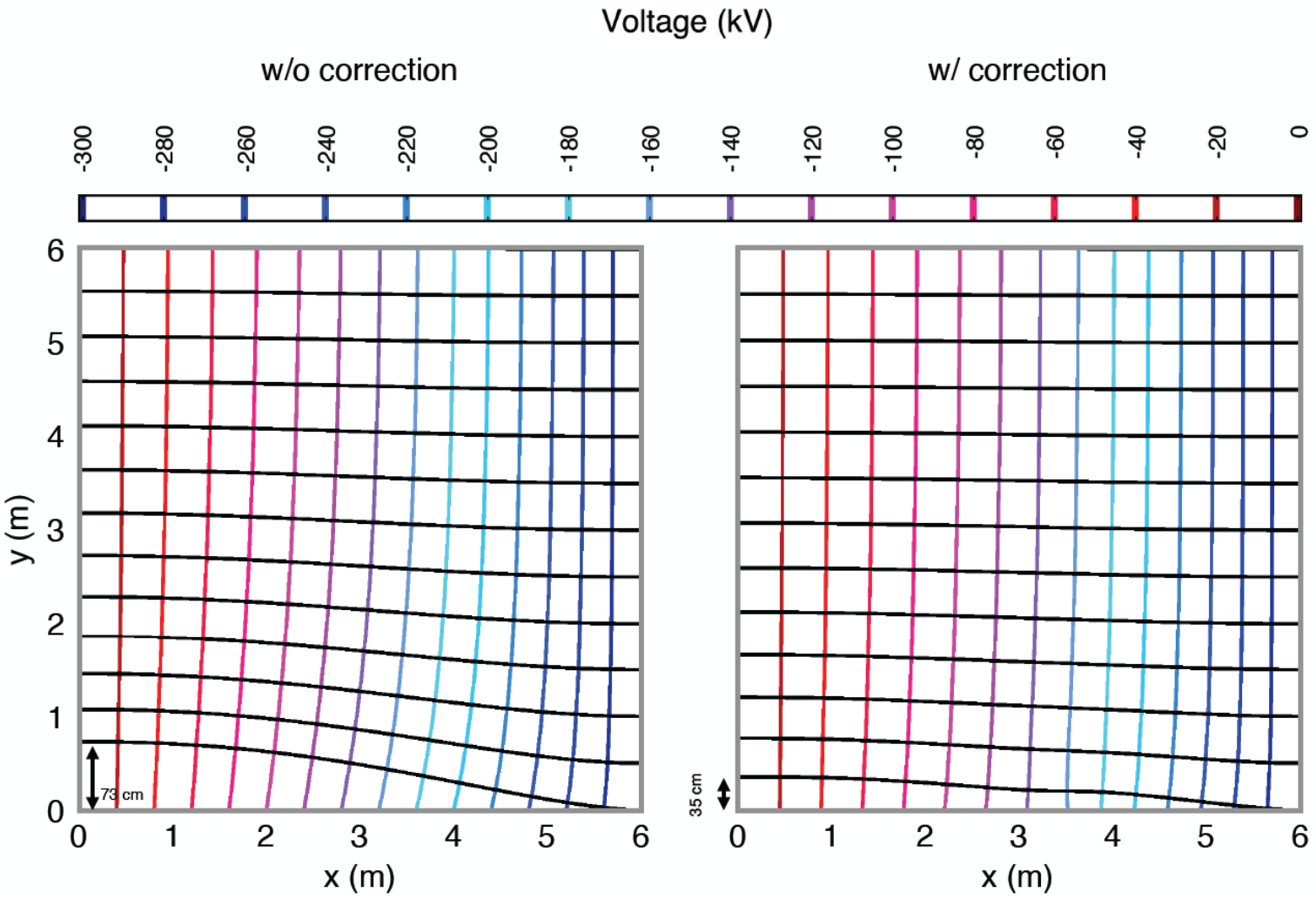

Numerical computation for 6 m TPC of large transversal size, on Earth surface, at 500 V/cm: equipotential surfaces and drift paths.

On the right plot, the field cage voltage profile has been modified with a third voltage connection, at x=3.5 m, set to cancel the transverse E field component at that position.

The maximum transversal distortion is reduced by a factor of 2.

Additional numerical studies

3D computations have been made, showing the the aspect ratio defines the interplay between longidudinal and transversal space charge distortions. Olso considered were the rather small effects due to

- initial recombination (E-field dependent),
- finite electron lifetime.

Note that effect of space charge on specific dE/dx measurement, for particle ID, enter via the effects on dQ for initial recombination, and on the distortion of dx (longitudinal and transversal).

A mitigation approach based on a grid, placed as a third electrode between anode and cathode, has been also considered. (ICARUS before ProtoDUNE.)

See reference for these subjects.

The effect of a grid, placed at x=0.75 L and with voltage V_g=0.75 V_0, in case of large/critical space charge conditions.

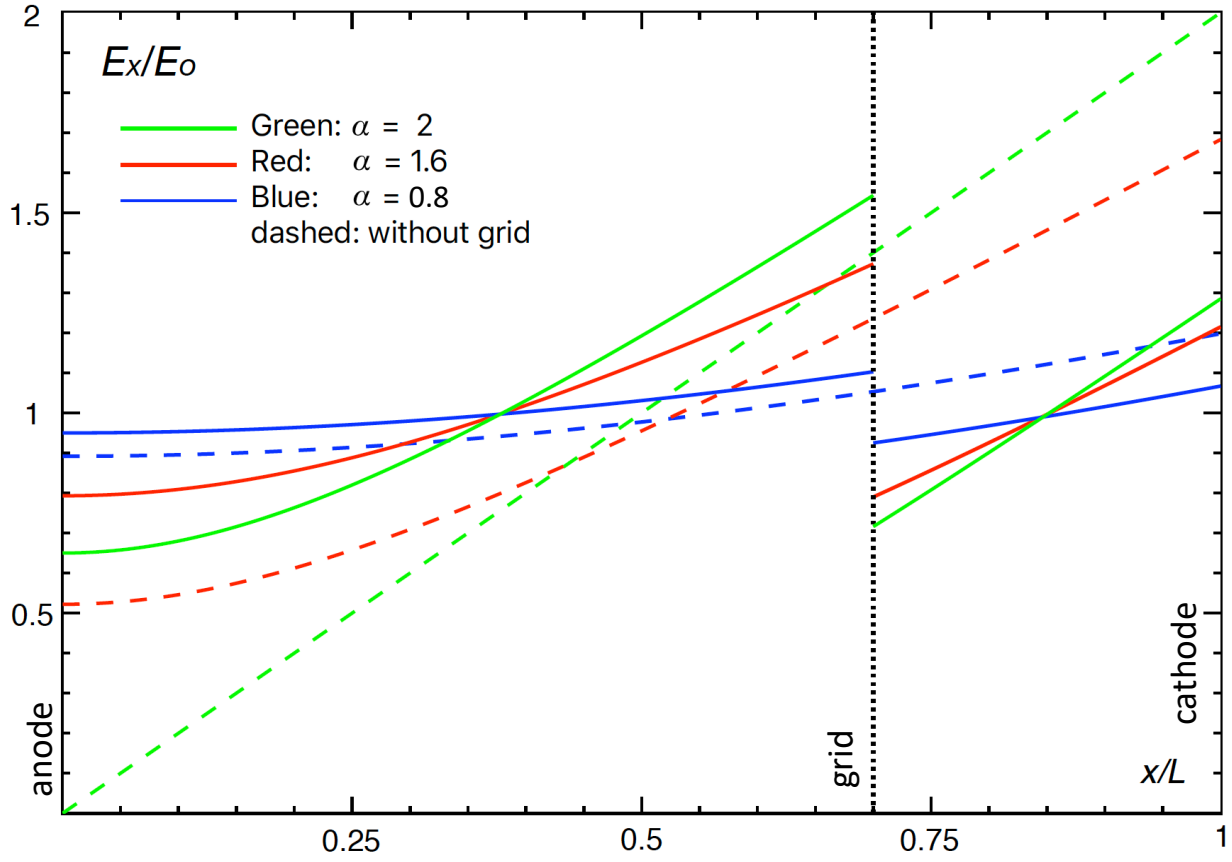

The case of dual-phase TPC with electron multiplication

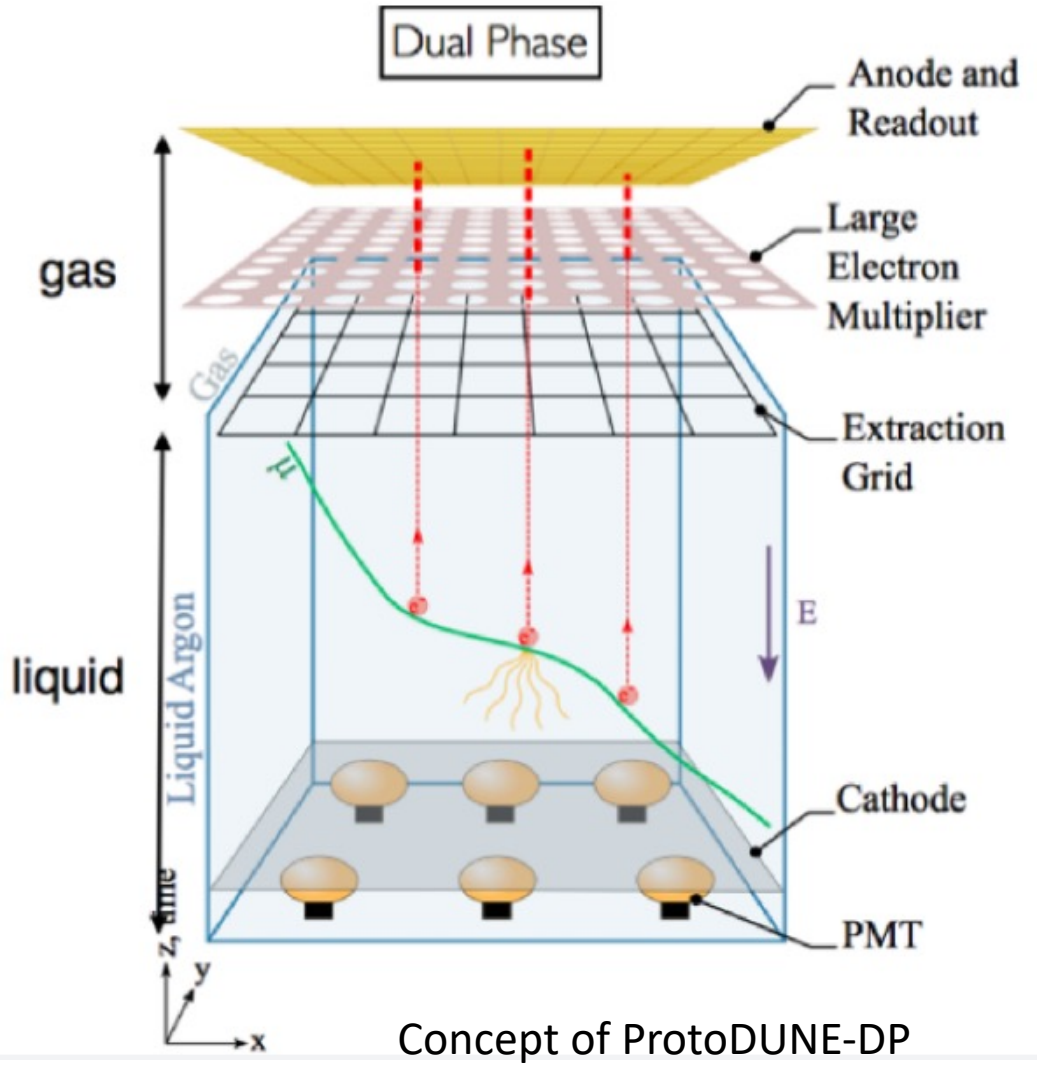

Concept of ProtoDUNE-DP

- If there is charge gain g in the gas, and positive ions are fed back to the liquid phase at a fraction f, then, with $\beta = f(g-1)$, the basic equation for the electric field becomes

$$E_x(x) = E_\circ \sqrt{(E_a/E_\circ)^2 + \alpha^2[(x/L)^2 + 2\,\beta\,(x/L)]}$$

- Limits of critical conditions can be read on the dependence of E_a on α and β:

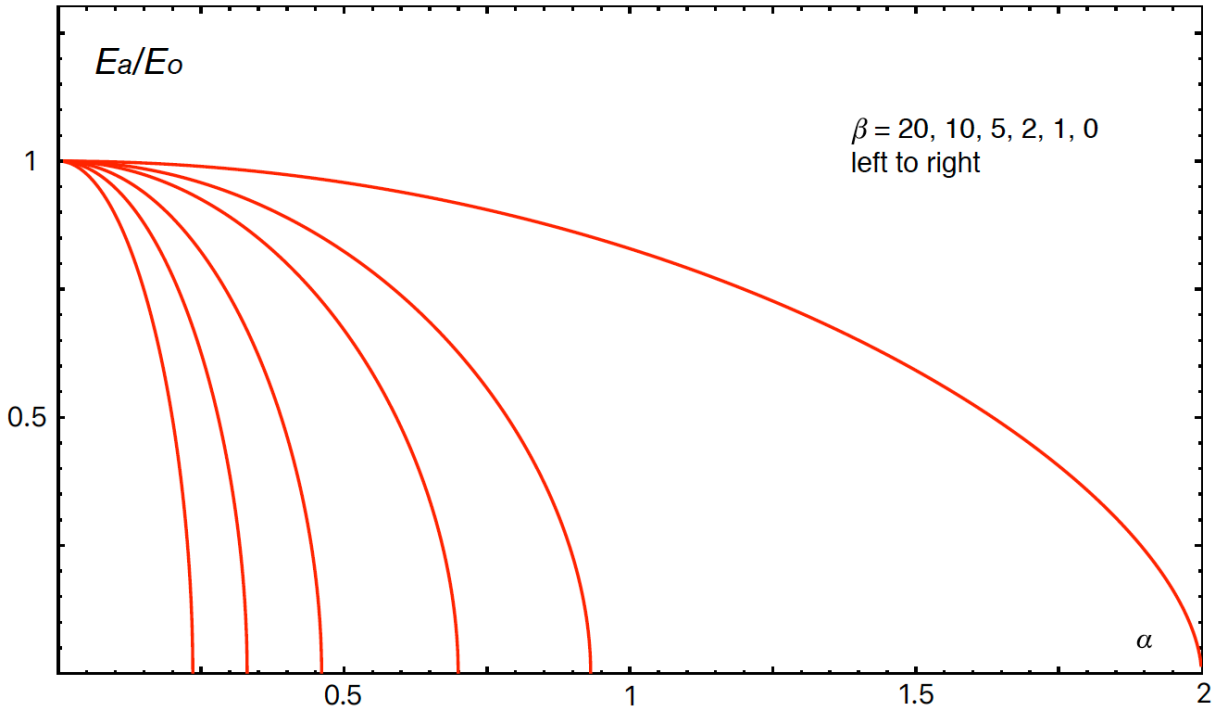

Another side subject: LKr TPCs ?

- Isotopic radioactivity in available krypton was not a concern for NA48, despite a relevant rate of about 500 Bq/cm^3, for an average energy of 250 keV from ^{85}Kr decays.
- It corresponds to a charge injection rate about 200 times smaller than the beam related value in the central part of the detector.
- However could we operate a LKr TPC, with gap of 0.5 m and electric field of 500 V/cm?
- With ion mobility as estimated by NA48 and the expectation for charge yield, for these gap and field values we obtain $\alpha \sim 10$. The answer therefore is **no**, one needs significantly lower gap and/or larger E field values.

- For comparison, argon radioactivity does not represent a concern – possibly with the exception of dual-phase large-gain devices for very long drifts gap.

But LAr TPCs may have further complexity

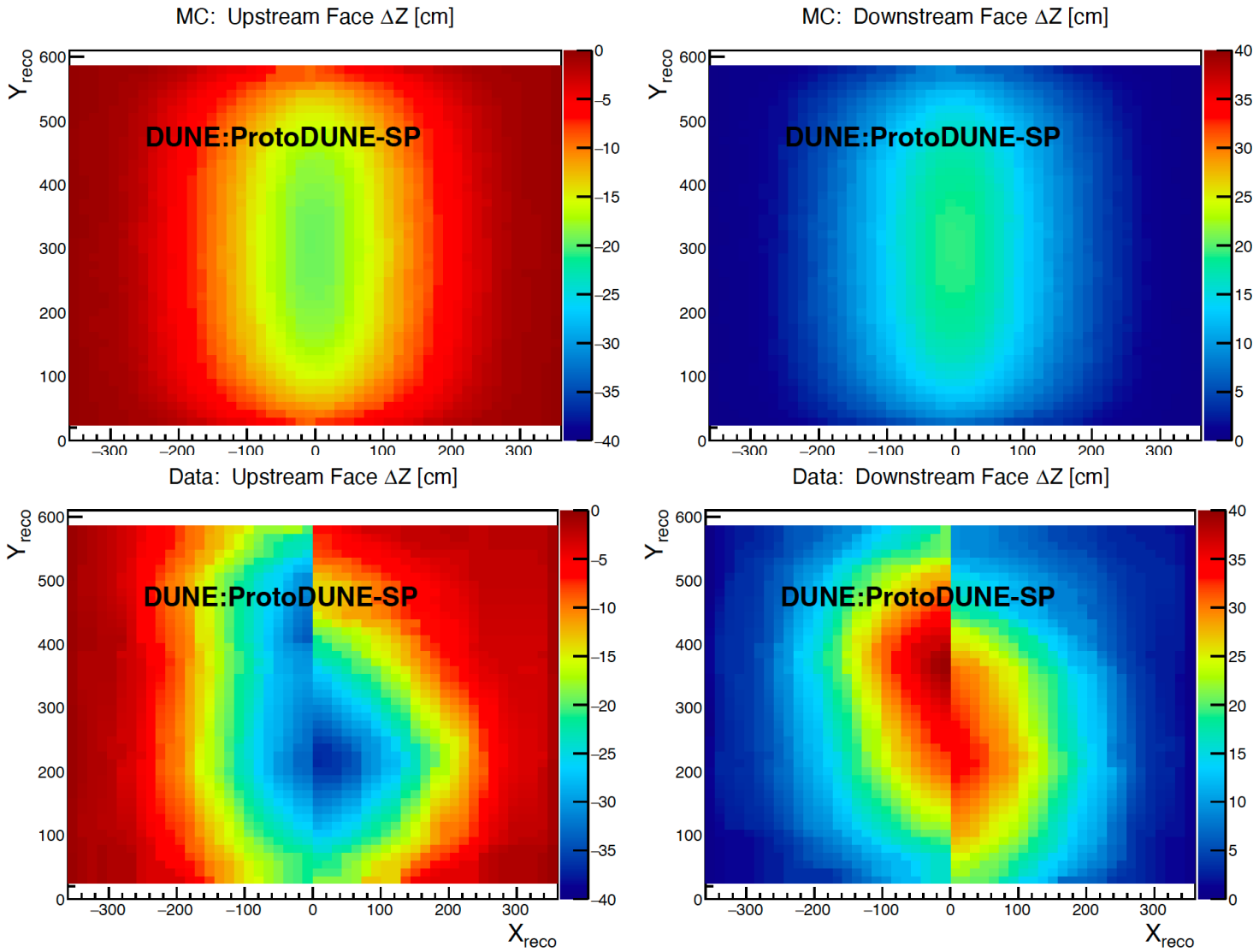

- The transversal distortions on the side boundaries are largest near the cathode, away from the other side walls.
- In this plots, both drift volumes are shown, with the cathodes in the middle.
- Data contain features similar to expectations, but typically larger, and asymmetric between top and bottom, and between the two drift volumes.

Fluid motion

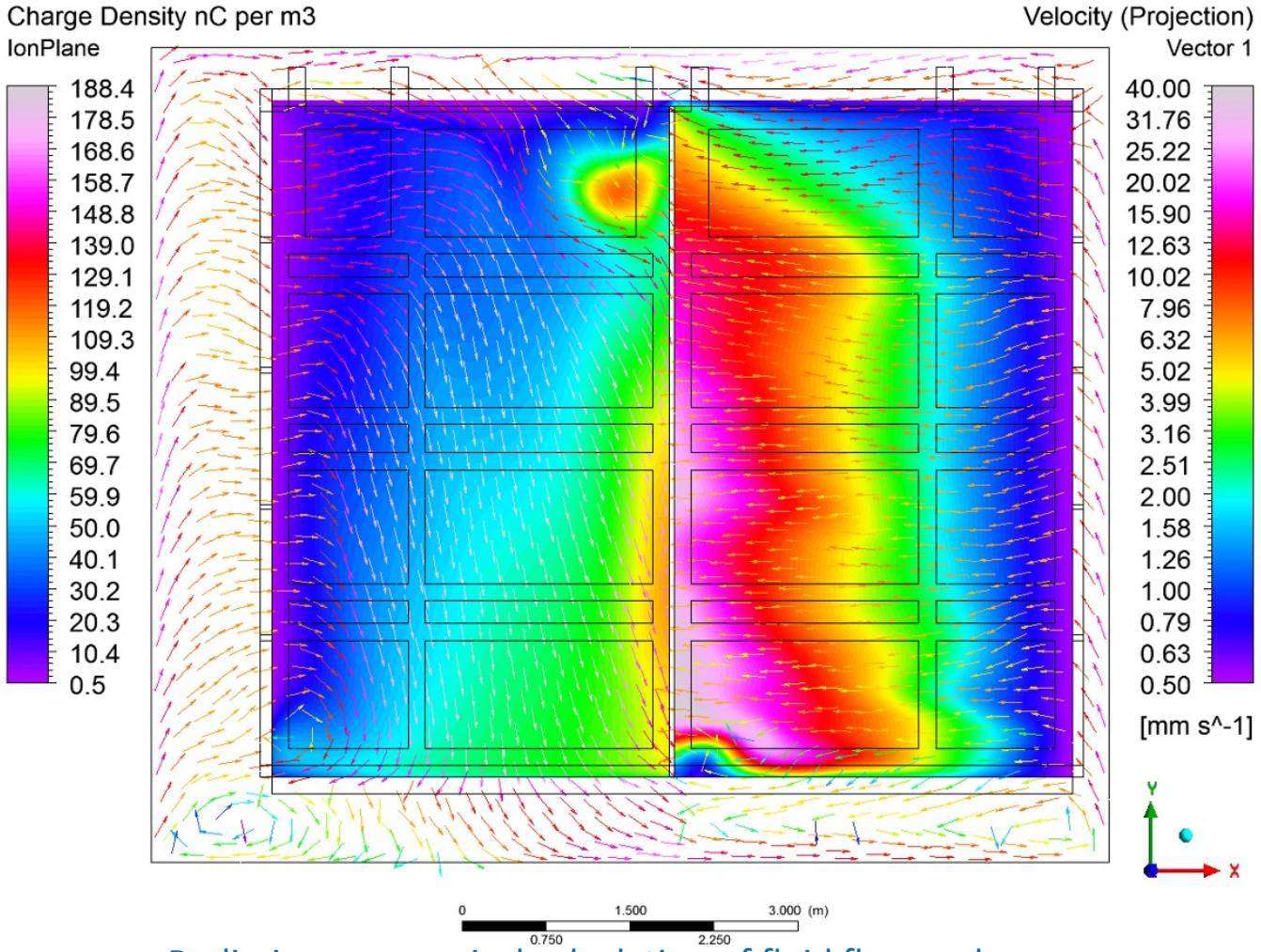

Preliminary numerical calculation of fluid flow and space charge, on the mid-plane z=0 of the ProtoDUNE-SP detector.

- In ProtoDUNE-SP, argon recirculation occurred as vapor and liquid, the latter at a rate of 7 ton/h, corresponding to a volume replacement every 5 days.
- The fluid motion (very successful in establishing an electron lifetime well above 10 ms), was highly asymmetric, due to number and location of inlet and outlets, and asymmetric location of the detector in the cryostat.
- The fluid flow has been computed to be mostly in the range of 1 to 15 mm/s, so it interferes significantly with the drift motion of ions, which is ~6 mm/s.
- The field cage, and the cathode (close membrane) contribute significantly to non-uniformity and asymmetry in the space charge density distribution.

Geometrical calibration

- Calibration devices: steerable laser beams can provide straight reference lines, and charge yield calibration pulses.
- Data driven methods con also contribute significantly to calibration:
  - Entrance point on side boundaries provide a reference value for transversal distortion (the distortion only occurs normal to the side wall).
  - The cathode crossing points provide the maximum drift time, constraining the cathode coordinate, but are not very sensitive to the longitudinal space effects along the drift gap.
  - Sidewall-anode, sidewall-sidewall and anode-(cathode)-anode crossing tracks provide a calibration track: the crossing point on the anodes are not displaced, and the apparent combined track can be directly compared to the segment connecting the end points.
  - There still remains some residual ambiguity in distinguishing the transversal and longitudinal components of the offset to the reference straight segment. That could be clarified by considering nearly intersecting tracks: since the (nearly) intersection points maintain the property after the distortion, they solve the ambiguity of the correction.

Data driven geometrical calibration

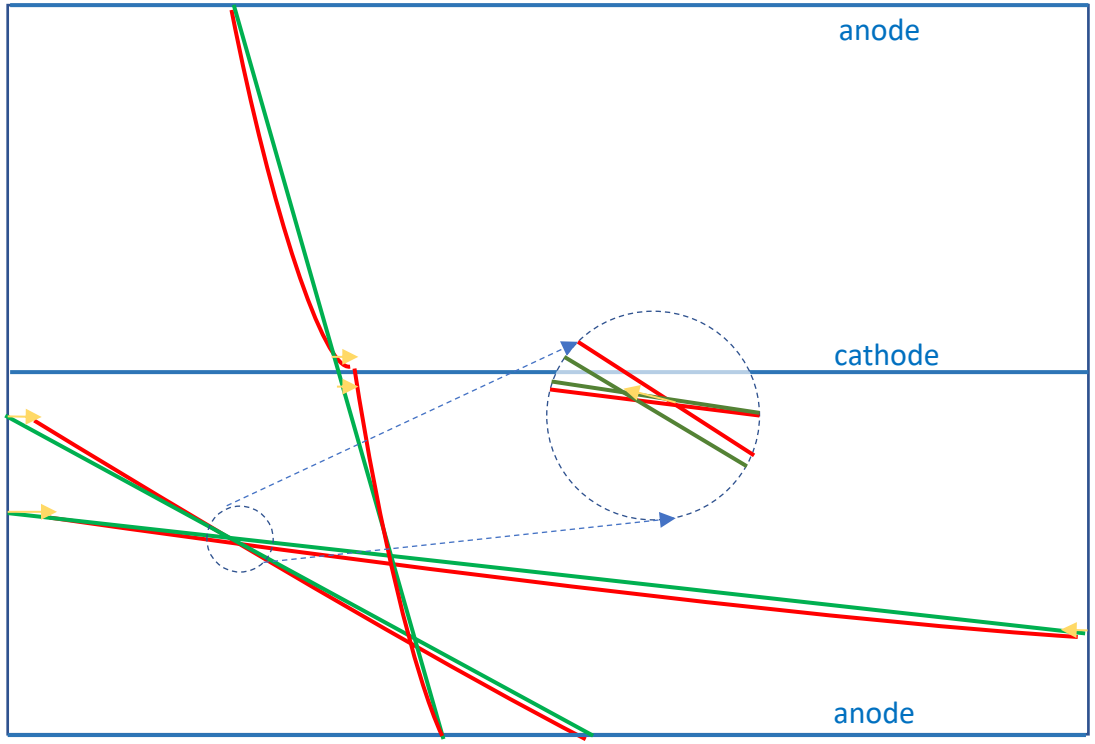

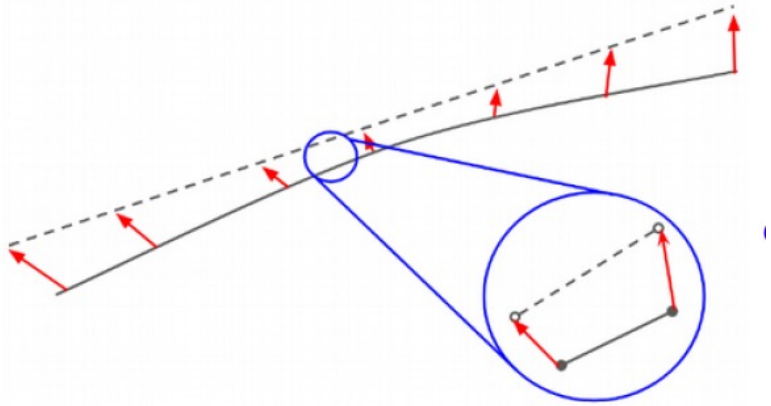

The (approximately) intersection allows for unambiguous point to point correction.

Conclusions

Where do we stand:

- The behaviour of calorimeters is understood, and detector design solutions can cope with very high intensity, by means of large HV and/or small gap values, in particular for sampling devices.
- LAr TPCs on Earth surface are affected by space to considerable (ProtoDUNE, MicroBooNE) or small (ICARUS, SBND) extent. Fluid flow adds complexity – its effect on space charge should not be neglected when designing recirculation schemes and rates. Space charge is not a concern for deep underground experiment.

References, acknowledgements

1. NA48 calorimeter, basic 1D model: S. Palestini et al., Space charge in ionization detectors and the NA48 electromagnetic calorimeter, Nucl. Instrum. Methods Phys. Res. A 421 (1999) 75.

2. ATLAS FCAL R&D: J.P. Rutherfoord and R.B. Walker, Space-charge effects in liquid argon ionization chambers, Nucl. Instrum. Methods Phys. Res. A 776 (2015) 65.

3. ProtoDUNE-SP: DUNE Collaboration, B. Abi et al., First results on ProtoDUNE-SP liquid argon time projection chamber performance from a beam test at the CERN Neutrino Platform, JINST 15 (2020) P12004 (arXiv:2007.06722).

4. ICARUS Collaboration, Antonello, M. et al. Study of space charge in the ICARUS T600 detector, JINST 15 (2020) P07001 (arXiv:2001.08934).

5. MicroBooNE: MicroBooNE Collaboration, Abratenko, P. et al. Measurement of space charge effects in the MicroBooNE LArTPC using cosmic muons, JINST 15 (2020) P12037 (arXiv:2008.09765).

6. 2D/3D models, mitigation approaches: Palestini, S. and Resnati, F. Space charge in liquid argon time-projection chambers: a review of analytical and numerical models, and mitigation method, JHEP 16 (2021) P01028 (arXiv:2008.10472).

7. DUAL-Phase TPC, ProtoDUNE-DP: DUNE Collaboration, B. Abi et al., “The DUNE Far Detector Interim Design Report, Volume 3: Dual-Phase Module,” arXiv:1807.10340 [physics.ins-det].

8. Computations of Fluid motion in ProtoDUNE-SP: E.A. Voirin, DUNE-Doc-928 (2019). See aklso S.z Tu, Ch. Jiang, T.R. Junk and T Yang, A numerical solver for investigating the space charge effect on the electric field inLAr TPCs, in preparation, on the extension of the basic model to include fluid motion.

9. On data driven TPC calibration: M. Mooney, Measurrment of space charge effects in ProtoDUNE-SP, ICHEP 2020, and private communications.

10. Review paper on this subject: S. Palestini, Space Charge Effects in Noble Liquid Calorimeters and Time Projection Chambers, Instruments 5 (2021) 1, 9, arXiv: 2102.06082 [physics.ins-det]

Acknowledgements: Thanks to Filippo Resnati, Flavio Cavanna, Milind Diwan, Kirk McDonald, Michael Mooney, Francesco Pietropaolo, Stephen Pordes, Tingjun Yang and Bo Yu for useful discussions on this subject.

Table 1
Physical properties of liquid krypton

Z	36
A	84
ρ (g/cm^3), density at 120 K	2.41
X_0 (cm), radiation length	4.7
R_M (cm), Molière radius	4.7
W (eV/pair), energy to create one ion–electron pair	20.5
λ_I (cm), nuclear interaction length	60
T_b (K), boiling point at 1 bar	119.8
T_m (K), melting point	116.0
v_d^e (mm/μs), electron drift velocity at 1(5) kV/cm	2.7 (3.7)
E_c (MeV), critical energy	21.51

Ion mobility $\mu = 0.45\ \mathrm{cm}^2\ \mathrm{kV}^{-1}\ \mathrm{s}^{-1}$

NA48: At maximum: K_{eff} = 130 pC cm^{-3}s^{-2}, or 8 10^8 ions cm^{-3}s^{-2}
Cfr. krypton radioativity of of 1.4 pC cm^{-3}s^{-2}

Intesity: 1100 GeV cm-2 s-1 in central region of the detector, 100 times less on outer boundary.

J.P. Rutherfoord, R.B. Walker / Nuclear Instruments and Methods in Physics Research A 776 (2015) 65–74

We have uniformly irradiated liquid argon ionization chambers with betas from high-activity ^{90}Sr sources. The radiation environment is similar to that in the liquid argon calorimeters which are part of the ATLAS detector installed at CERN's Large Hadron Collider (LHC). We measured the resulting ionization current over a wide range of applied potential for two different source activities and for three different chamber gaps. These studies provide operating experience at exceptionally high ionization rates. In particular they indicate a stability at the 0.1% level for these calorimeters over years of operation at the full LHC luminosity when operated in the normal mode at an electric field $\mathcal{E} = 1.0$ kV/mm. We can operate these chambers in the normal mode or in the space-charge limited regime and thereby determine the transition point between the two. This transition point is parameterized by a positive argon ion mobility of $\mu_+ = 0.08 \pm 0.02$ mm^2/V s at a temperature of 88.0 ± 0.5 K and at a pressure of 1.02 ± 0.02 bar. In the space-charge limited regime the ionization currents are degraded and show signs of instability. At the highest electric fields in our study (6.7 kV/mm) the ionization current is still slowly rising with increasing electric field.